Received: 21 July 2020 | Revised: 21 December 2020 | Accepted: 26 February 2021

DOI: 10.1002/joc.7082

RESEARCH ARTICLE

International Journal of Climatology RMetS

# Long-term evolution of global sea surface temperature trend

Zhenhao Xu[1] | Fei Ji[1,2] | Bo Liu[3] | Taichen Feng[1] | Yuan Gao[1] | Yongli He[1,2] | Fei Chang[4]

[1]College of Atmospheric Sciences, Lanzhou University, Lanzhou, China

[2]Collaborative Innovation Center for Western Ecological Safety, Lanzhou University, Lanzhou, China

[3]School of Information Science and Engineering, Lanzhou University, Lanzhou, China

[4]Gansu Air Traffic Management Sub-bureau of CAAC, Lanzhou, China

**Correspondence**
Fei Ji, College of Atmospheric Sciences, Lanzhou University, Lanzhou, China.
Email: jif@lzu.edu.cn

**Funding information**
Chinese Desert Meteorological Science Research Found, Grant/Award Number: Sqj2019013; National Natural Science Foundation of China, Grant/Award Numbers: 41705047, 41875083, 42075029

**Abstract**

The ocean plays an essential role in regulating global and regional climate, which is mainly achieved through sea surface temperature anomaly (SSTA) changes. Studies on global sea surface temperature (GSST) are primarily carried out under linear assumption, which is not capable of fully revealing the evolution characteristics of sea surface temperature (SST) due to the non-linear and non-stationary nature of the SST. Here, the evolution of the GSST trend in the past century is investigated by using an adaptive and local spatial–temporally multidimensional ensemble empirical mode decomposition method. The results show that the global ocean has been warming except for the subpolar North Atlantic, the equatorial central Pacific, and the Southern Ocean in the Pacific sector. The equatorial central Pacific turned from cooling to warming around the middle of the last century made it one of the fastest-warming regions in recent decades with other regions located in the Arctic Ocean and the western-boundary current regions and their mid-latitude extensions in both hemispheres. The strongest warming during recent decades is found in the Arctic Ocean, east of the continents in the northern hemisphere, the entire Indian Ocean, and especially in the tropical Pacific Ocean. From a zonal average perspective, warming (>0.1 K since 1900) first took place in the subtropical regions of the Northern Hemisphere and 50°S of the Southern Hemisphere almost simultaneously around 1910, then followed by the subpolar warming in the Northern Hemisphere. The first two bands of warming both expanded equatorward leading to the fast warming of tropical oceans, especially for the Pacific Ocean.

**KEYWORDS**

centennial trend, evolution, global sea surface temperature, MEEMD

## 1 | INTRODUCTION

The increased and accumulated human-emitted greenhouse gases (GHGs) in the atmosphere have resulted in the long-term warming of the Earth. Over the twentieth century, the annual-mean globally averaged surface temperature has risen about 0.89°C (IPCC, 2013), and the warming is projected continuation in the future (Meehl *et al.*, 2007).

The global ocean comprises the bulk of the hydrosphere, covering over 70% of Earth's surface. Because oceans have hundreds of times more mass than the

  

atmosphere, and therefore large heat-storage capacity and very high thermal inertia, the oceans play several critical roles in the climate system. These roles are related to the key physical properties of the ocean. In addition to the direct physical effects, the global ocean can affect the climate system indirectly through chemical and biological processes. Meanwhile, the ocean and atmosphere can also work together to spontaneously generate internal climate variability that can persist for years to decades at a time (Brown *et al*., 2015), such as the El Niño–Southern Oscillation (ENSO), the Pacific decadal oscillation (PDO), and the Atlantic Multidecadal Oscillation (AMO). Generally, the aforementioned processes including ocean currents, the thermohaline circulation, exchange of gases across the air-sea interface, and the internal climate variability generated by ocean–atmosphere coupling can greatly affect Earth's climate by transferring heat from the tropics to the polar regions, redistributing heat between the deep ocean and the atmosphere, and also by altering the cloud, water vapour, or sea ice distribution, which can ultimately affect the total energy budget of the earth. So, understanding the ocean processes is a necessary part of understanding climate and helping scientists to attribute recent climate change. (Trenberth *et al*., 2014).

The global climate has been experiencing critical long-term warming by human-caused GHGs at an extraordinary pace in the past century, which is known as 'global warming' (IPCC, 2013). As the principal component of Earth's hydrosphere, the global ocean is reported to store more than 90% of the excess heat, and the mean ocean surface temperature has been observed long-term warming since the mid-19th century (IPCC, 2019). Cheng *et al*. (2020) also confirmed that the world's oceans (especially at upper 2000 m) in 2019 were the warmest in recorded human history measured by ocean heat content (OHC) data. The environmental effects of warming are broad and far-reaching, and many impacts are already visible. For example, the global mean sea level has been rising, with an acceleration detected as well, and is expected to accelerate further over the coming century (Chen *et al*., 2017b). The rise of current and future sea level rise has a number of impacts, particularly on coastal systems, and the number of people who will be impacted by sea level rise during the 21st century is three times higher than that was previously thought (Kulp and Strauss, 2019). Oceans worldwide are undergoing acidification caused by the uptake of carbon dioxide (CO2) from the atmosphere (Cai *et al*., 2011), and deep oceans may acidify faster due to global warming (Chen *et al*., 2017a). One of the effects of ocean acidification called coral bleaching can be seen on the Great Barrier Reef in Australia, where ocean acidification's effects are already taking place. Increased acidity presents a threat to the food chain and ecosystem, and can seriously harm the fishing industry of the global economy. Another effect is ocean deoxygenation, which is projected to increase hypoxia by 10% for each 1°C of upper ocean warming (Deutsch *et al*., 2011). Global ocean warming also affects weather patterns as they pertain to cyclones (Webster *et al*., 2005), changing the number of hazards on the ocean, and causing the ocean to create more floods due to the sea level rise. Overall, the ongoing global warming has various effects on oceans and triggers several changes in the ocean, all of which bring risks and opportunities to ecosystems and people. It implies all people on Earth depend directly or indirectly on the ocean (IPCC, 2019), and more evidence and understanding of ocean changes under a warm climate is necessary for mitigation, adaptation, and governance options to reduce future risks.

The oceans play essential roles in the energy budget of the climate system. The energy fluxes exchanged at the sea surface depend on the SST, as well as several atmospheric parameters (Deser *et al*., 2010a). SSTs thus play a key role in regulating climate and its variability and are well suited for monitoring climate change. A majority of researches studied the characteristics of the global ocean or oceanic divisions mostly from reconstructed data sets, and most of which have focused largely on SST long-term trends (Deser *et al*., 2010b). Discrepancies are found from various data sets with different coverage and quality of in situ observations in the centennial record (Giese *et al*., 2010); nevertheless, some features in common are well established. Deser *et al*. (2010b) evaluated 20th century SST trends from a variety of data sources including un-interpolated archives as well as globally complete reconstructions and found that global oceans warmed almost everywhere except the northern North Atlantic while the tropical Pacific SST responded to global warming would be an 'El Nino-like' or a 'La Lina-like' pattern. Globally SST data sets are becoming more and more accurate with the improved analysis methods and utility of satellite remote sensing data, which allows better analysis of SSTs.

To study how the GSST's centennial trend has evolved since 1900, we investigate the time-varying intrinsic trend in GSST by an adaptive data analysis approach. Traditionally used linear trend method often requires a priori linear form assumption and is subject to the time interval selection, which is often based on an arbitrary decision. Unlikely, Wu *et al*. (2007) defined an intrinsic trend as 'an intrinsically fitted monotonic function or a function in which there can be at most one extremum within a given data span'. The method we take advantage of to

derive spatial–temporally varying trend is the multi-dimensional ensemble empirical mode decomposition (MEEMD; Wu *et al*., 2009), a method based on ensemble empirical mode decomposition (EEMD; Huang *et al*., 1998; Huang and Wu, 2008; Wu and Huang, 2009), which is a local and adaptive analysis of nonlinear and non-stationary time series (see Section 2 for more information). Both EEMD and MEEMD have been widely applied in climate research (Franzke, 2009; Qian *et al*., 2010; Hu *et al*., 2012; Ji *et al*., 2014) and they will favour detailing how the SSTs respond to global warming in a centennial timescale. Especially, Wang *et al*. (2014) proved that the time complexity of the EEMD is actually equivalent to the Fourier Transform, which provides a strong guarantee for large-scale data calculation.

## 2 | DATA AND METHOD

### 2.1 | Data

Accurate determination of long-term SST trends is always suffering from considerable data uncertainty, which limits the physical interpretation and utility as verification for climate model simulations. Deser *et al*. (2010b) evaluated 20th century SST trends by comparing results from a variety of data sources including un-interpolated archives as well as globally complete reconstructions. They found all datasets were generally similar by showing consistency in the statistically significant trends except for the equatorial eastern Pacific.

In this study, the monthly extended reconstructed sea surface temperature version 5 dataset (ERSSTv5) over the global ocean from January 1900 to December 2016 is analysed. ERSSTv5 represents an improvement upon the previous version ERSSTv4 in source data sets used and in key aspects of quality control, homogenization, and interpolation (Huang *et al*., 2017a; 2017b). This dataset has $2^\circ \times 2^\circ$ spatial resolution. Here we also compared results from three other most commonly used SST data sets in climate studies, including COBE-SST (Ishii *et al*., 2005) at Japan Meteorological Agency (JMA); Hadley Centre sea ice and SST version 1 (HadISST1) (Rayner *et al*., 2003), and Kaplan Extended SST version 2 (Kaplan v2) (Kaplan *et al*., 1998) which are listed in Table S1 of Supporting Information and our discussion is limited to those data sets.

### 2.2 | The EEMD

In this article, we use the MEEMD method to study the evolution of warming in GSST's centennial trend. This method is developed based on the EEMD method, which is suitable for adaptive analysis of nonlinear and non-stationary time series and is particularly powerful in extracting low-frequency components and the intrinsic secular trend from complex climate data (Wu *et al*., 2007). These methods have already been widely used in the climatic and oceanic analysis. Here we briefly introduce the method and the detailed procedures can be found in previous studies (Huang *et al*., 1998; Huang and Wu, 2008; Wu and Huang, 2009).

In EEMD, a time series $x(t)$ is decomposed into a set of amplitude–frequency-modulated oscillatory components (intrinsic mode functions, IMFs) $C_j(t)$, $j = 1,2, \ldots n$ and a residual R(t): $x(t) = \sum_{j=1}^{n} c_j(t) + R(t)$. In this article, we use the white noise with variance $\sigma = 0.2$ relative to the variance of the raw data, and $N = 400$ ensemble members.

By the decomposition, a time series can be separated into signals with different timescales including annual cycle, interannual, decadal, multidecadal variabilities, and a secular trend, while previous applications of the EEMD method were focusing on particular components (Wu *et al*., 2011; Ji *et al*., 2014; Wei *et al*., 2019). Here, we are interested in the centennial-scale ocean warming represents by $R(t)$, which is defined as a curve either monotonic or containing only one extremum from which no additional oscillatory components can be extracted.

The time-varying nature of the intrinsic trend defined above provides a new perspective for the trend analysis. Following Ji *et al*. (2014), we define the EEMD trend of a SST series as $\mathrm{Trend}_{\mathrm{EEMD}}(t) = R(t) - R(1900)$, representing the ocean's accumulated warming from 1900. For multi-dimensional spatial–temporal GSST data, we piece together $R(t)$s from all grids to form entire pictures of EEMD trends at the centennial timescale. This will provide more detailed information on how GSST's intrinsic trend has evolved during the last century, compared with a traditional time-unvarying linear method.

### 2.3 | Significant test of the EEMD components

EEMD decomposes a time series in terms of a set of components from high frequency to low frequency (IMFs), and a remainder (secular trend), which varies on timescales longer than the longest timescale of any oscillatory component. Do the IMFs and secular trend extracted by EEMD contain significant signals that can be distinguished from background noise? To answer this question, we discuss first the general concept of statistical significance of a component of a time series extracted by EEMD.

### 2.3.1 | Significant test of the IMFs

For IMFs extracted by the EEMD method, Wu and Huang (2004) proposed a test method for noisy data by implementing numerical experiments on white noise time series. They found that the product of the energy density ($\bar{E}_k$) of IMFs and the corresponding averaged period ($\bar{T}_k$) of IMFs is a constant: $ln\bar{E}_k + \ln\{\bar{T}_k\} = const$. It is also found that all the IMFs of white noise have normal distribution and the energy-density function of an IMF sample is $\chi^2$ distributed. They further established a test method to assign the statistical significance of any EEMD component which is applied in this article.

### 2.3.2 | Significant test of the secular trend

To test the statistical significance of the intrinsic secular trend, we used an approach developed based on a Monte Carlo method for testing the time-varying trend derived by the EEMD method (Ji *et al.*, 2014). For each grid with time-varying secular trend R(t) derived by the EEMD method, the general procedures of the statistical significance test are introduced as follows: (1) calculating the lag − 1 autocorrelation $\alpha$ of the yearly SSTA at each grid; (2) generating 5,000 random samples of red noise time series with the same temporal data length (117) and the lag − 1 autocorrelation $\alpha$ (if $\alpha = 0$ then the null hypothesis applied is white noise) at each gird; (3) deriving the secular trend of each generated red noise time series by the EEMD method; (4) comparing the standardized EEMD trend of the SST with the two-standard-deviation spread value of the trends of the red noise time series (around 95% of confidence) at any temporal locations at each gird. If the EEMD trend of SST falls outside the two-standard-deviation spread of the mean, it is considered statistically significant. Clearly, for the same value of EEMD trends at different locations, whether the value is statistically significant depends on both spatial and temporal locations.

## 2.4 | Estimation of the uncertainty of the secular trend

The down sampling approach (Wu *et al.*, 2011) is applied to estimate the uncertainties of the secular trend extracted by the EEMD method. Taking tropical central and eastern Pacific as an example, we randomly pick a value of the monthly mean SST of this area for each calendar year to represent the entire annual average, which leads to a yearly down-sampled GSST series. Theoretically, this approach could yield $12^{117}$ different time series. We then randomly choose 400 series and compute their secular trend by the EEMD method, and the corresponding spread of the trends provides the confidence interval.

# 3 | RESULTS

## 3.1 | Evolution of the GSST

There are several dominant patterns of nonseasonal SST variability in each ocean basin, as exemplified by the ENSO phenomenon in the tropical Pacific; the tropical Indian Ocean dipole mode (IOD); the PDO; and the AMO, with timescales from interannual to multidecadal, which influence regional climates and their variability worldwide. These primary modes of SST variability are always considered to be natural. By removing any variability on shorter timescales than the length of time series we studied, the residual one is regarded as the intrinsic trend like defined before. This component is also what we care about in this study, which will provide more detailed information on how the GSST has evolved under global warming within the given time span, compared with a typical linearly fitted approach. The spatial evolution of the accumulated warming of ocean is shown in Figure 1.

Before 1910, noticeable accumulated changes (>0.3 K or <−0.3 K) seemed to be sporadically distributed with slight cooling occurred in the equatorial central Pacific and the Southern Ocean in the Pacific sector, while east Greenland, the middle and eastern tropical Atlantic Ocean, and southwest of Indian Ocean warmed a little bit. The earlier sporadic cooling and warming both then have been expanding since 1925, meanwhile, warming over most of North Pacific and tropical Atlantic oceans and cooling over subpolar North Atlantic emerged. After 1955, one of the most remarkable phenomena is that areas of the first cooling regions including the equatorial central Pacific and the Southern Ocean begin to shrink, which means the EEMD trends over these regions are not monotonic. One of the benefits by using EEMD is that it can demonstrate how the centennial trends evolve during the time span. The nonlinear EEMD trends at different grids may change monotonically or have only one extremum by the definition. This unique nature may reveal some undiscovered features and be important even in the slightest hint for understanding global climate change. As exhibited in Figure 1, centennial trends over the equatorial central Pacific and the Southern Ocean in the Pacific sector both experienced two stages, one is cooling over the first half of the last century, the other is

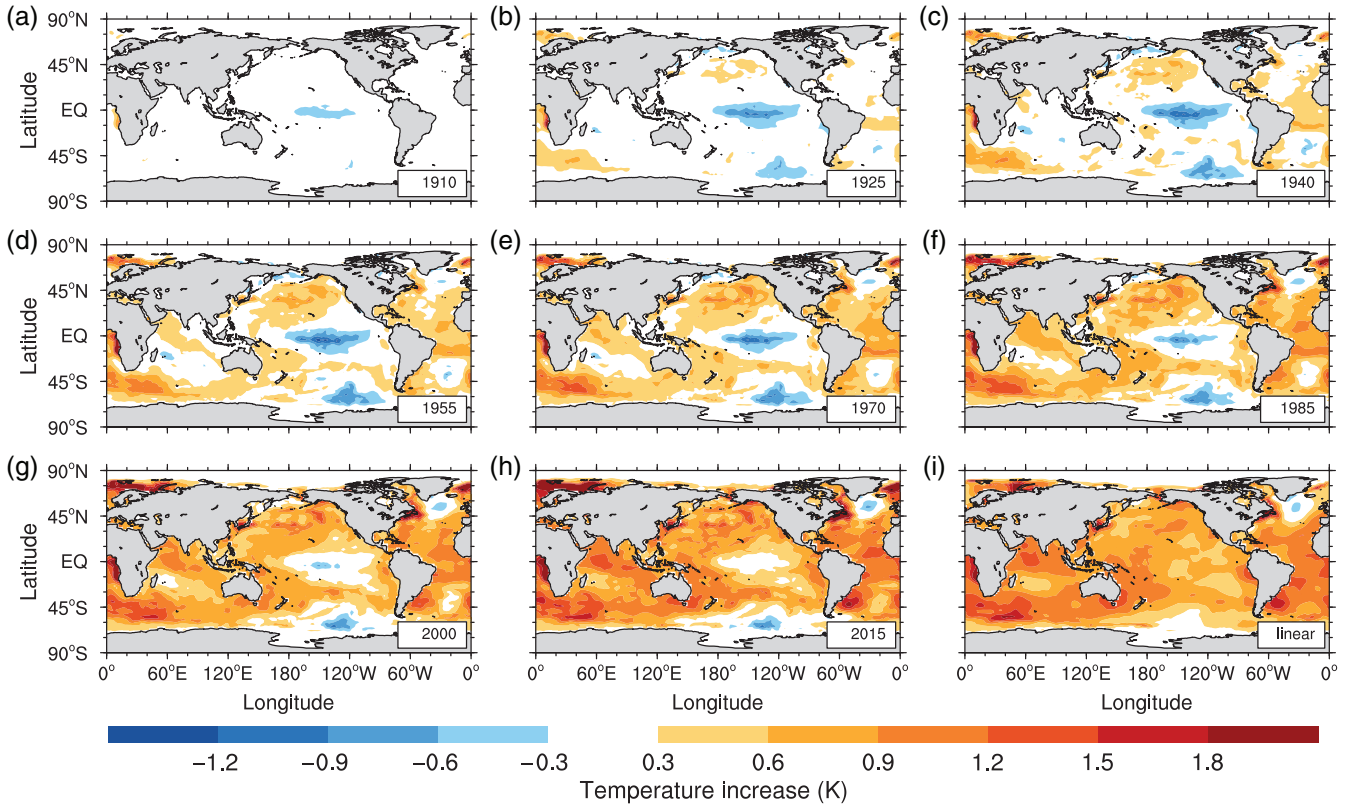


**FIGURE 1** Spatial evolution of the EEMD trend of global sea surface temperature. (a–h) EEMD trend ending in 1910, 1925, 1940, 1955, 1970, 1985, 2000, and 2015, respectively. (i) The spatial structure of temperature increase based on time-unvarying linear trend over the whole data domain from 1900 to 2015 [Colour figure can be viewed at wileyonlinelibrary.com]

warming during recent decades, which may also imply why there is a long-standing debate in the climate community as to how the tropical Pacific will respond to global warming: will it be an El Niño or a La Niña like pattern? (Zhang and Song, 2006; Vecchi *et al*., 2008).

The other advantage of the EEMD method is that it cannot only tell us how much has the temperature changed, but also places where temperature changed first. Generally, as we can find from Figure 1, the noticeable change of SSTs under global warming is located in the equatorial central Pacific with a cooling trend. Changes of SSTs over other oceans without the Indian Ocean then followed. From this perspective, it is clear that SSTs over different oceans change with different paces, while the equatorial central Pacific taking the lead and the Indian Ocean is the slowest. When focusing on the Indian Ocean, warming in the western Indian Ocean is greater than the eastern, which is consistent with the findings that the frequency and intensity of positive IOD events increased during the twentieth century (Abram *et al*., 2008, 2020) and associated with Australia's worst droughts (Ummenhofer *et al*., 2009), as well as wildfire risk and habitat destruction in Indonesia and southeast Australia (Cai *et al*., 2009).

GSST's EEMD trend in 2015 as shown in Figure 1h exhibits warming everywhere except the western of northern North Atlantic, the equatorial central Pacific, and the Southern Ocean. Despite the values of the EEMD trends in 2015 in these regions are negative, the detailed evolution features are different: the equatorial central Pacific and the Southern Ocean underwent a cooling before 1955 and warmed afterwards while cooling over the western of northern North Atlantic is sustained on a centennial scale. The greatest warming occurs over the Arctic Ocean, east of the continents in the northern hemisphere, and the eastern tropical Atlantic Ocean. The amplitude and spatial patterns of EEMD trends from 1900 to 2015 roughly resemble that of the linear trend over the same time span. However, the minute details of the evolution of GSST's warming pattern cannot be revealed by the linear trend (Figure 1).

## 3.2 | Warming rate of the GSST

Since the remainder of the MEEMD decomposition varies with time and space, the rate of warming/cooling obtained by calculating the slope of the trend at a given

time also has the properties of varying with time and space, which would be a useful approach to quantify the magnitude and spatial distribution of SSTs' changing rate. The instantaneous warming rate is determined by calculating the temporal derivatives of the EEMD trends. For example, the warming rate at 1910 is expressed as (EEMD trend at 1911–1909)/2, which are presented in Figure 2. Before 1910, there were both noticeable rapid warming and cooling regions. Warming occurred in the Arctic Ocean, North Pacific Ocean, tropical Atlantic Ocean and the Southern Ocean from the tip of South Africa expanded into both the Indian Ocean and the Atlantic Ocean, while cooling regions located in the equatorial central Pacific, the Southern Ocean, the South Indian Ocean, the North and South Atlantic Ocean. With the exception of subpolar North Atlantic, the cooling regions then shrank and most of them turned into weak warming regions over the next four and five decades. Meanwhile, deceleration took place in previously warming regions except for the Arctic. By 1970, except for the weak cooling in North Pacific, subpolar North Atlantic, and some isolated areas over the Southern Ocean and South Atlantic, almost all the global oceans had been warming. The spatial structure of the warming rates over global oceans has changed little since 1985, but with an accelerated pace of warming over the next decades.

The strongest warming during recent decades is found in the Arctic Ocean, east of the continents in the northern hemisphere, the entire Indian Ocean, and especially in the tropical Pacific Ocean. Warming over the Arctic Ocean maintained a high speed all the time corresponding to a phenomenon which is well known as 'polar or Arctic amplification'. Mechanisms have been proposed to explain this rapid Arctic warming, including snow- and ice-albedo feedback (Screen *et al*., 2012), local radiative effects from increased greenhouse-gas forcing (Stroeve *et al*., 2012), changes in aerosol concentration, Arctic cloud cover, and several other processes (Cohen *et al*., 2014). Other conspicuous regions in the extra tropics that stand out as having the strongest warming are the western-boundary current regions and their mid-latitude extensions in both hemispheres including the Kuroshio current, the Gulf stream, the Eastern Australian Current, the Brazil Current, and the Agulhas Current. This enhanced warming over the global subtropical western boundary currents in the twentieth century is found might be attributable to the poleward shift

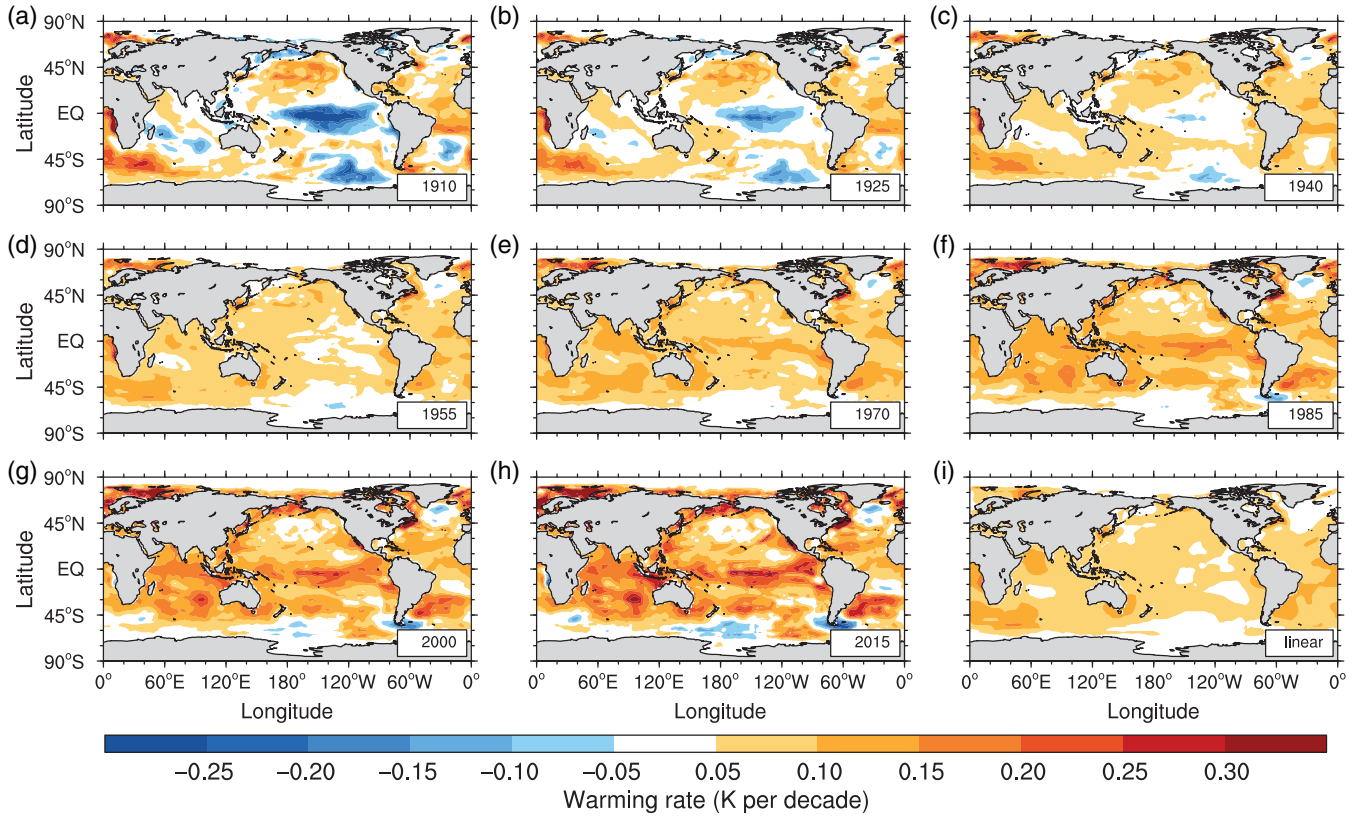


**FIGURE 2** Warming rate of global sea surface temperature. (a–h) The instantaneous warming rate of the secular trend in 1910, 1925, 1940, 1955, 1970, 1985, 2000, and 2015, respectively. (i) The spatial structure of the warming rate based on the time-unvarying linear trend over the whole data domain from 1900 to 2015 [Colour figure can be viewed at wileyonlinelibrary.com]

of their mid-latitude extensions and/or intensification in their strength and may reduce the ability of the oceans to absorb anthropogenic carbon dioxide over these regions (Wu *et al*., 2012). For the Indian Ocean, the spatial pattern of warming/cooling rates evolved from a north–south dipole mode to a basin-wide mode. The former is illustrated by weak warming in the northwest and moderate cooling in the south Indian Ocean, respectively. Warming then expanded slowly in the next few decades while cooling regions shrank and turned into warming regions. The entire Indian Ocean warmed with an accelerated pace of warming in recent decades. Combined with Figure 1, it is also found that the centennial-scale warming trend over the western Indian Ocean surpassed that over the warm pool in both magnitude and period. Consistent with previous studies, the warming of the generally cool western Indian Ocean against the rest of the tropical warm pool region was found could change the zonal SST gradients, and had potential effects on the Asian monsoon circulation and rainfall, as well as altered the marine food webs in this biologically productive region (Roxy *et al*., 2014). As far as the Pacific Ocean and the Southern Ocean are concerned, the initial rapid warming in the north Pacific, fast cooling in the equatorial central Pacific and the Southern Ocean all underwent remarkable deceleration during the first decades of the last century. Since 1970, warming rates over North Pacific have been flattened and turned into sporadically distributed weak cooling rates after 2000. At the same time, dramatic changes have taken place in the equatorial central Pacific and the Southern Ocean, initially, cooling trends turned into rapid warming with accelerated paces during recent decades.

The evolution of the GSST's centennial trend and warming/cooling rate derived by the EEMD method give scientists new insights into where and when the SSTs started to warm and how warming/cooling rates changed over time. Generally, the equatorial central Pacific Ocean experienced the most dramatic changes during the last century. EEMD trends of 2015 in the equatorial central Pacific are still negative though the strongest warming is found to occur in this region, which may be mainly due to the local long-term low SSTs caused by equatorial and coastal upwelling. Another noticeable feature is that it is a relatively gentle period from 1950 to 1970 no matter for warming or cooling regions corresponding to the mid-twentieth-century cooling period of global warming (Yao *et al*., 2017). The spatial structure of the warming rate obtained from linear fitting resembles that from the EEMD method at 1955, demonstrating moderate global warming. For the limitation of the linear method, it only captures the mean state of the warming rate while the most attractive but opposite changes at first and last decades have been averaged.

## 3.3 | Zonally averaged trend

In order to obtain the main features of the spatial–temporal evolution of the warming, the zonally averaged trends of global oceans are plotted in Figure 3. We applied a running mean over the range of 5° in meridional direction and 3 years in time axis to eliminate the noisy pattern generated by sporadic warming/cooling.

The zonally averaged land surface air temperature warming is found to have a three-band structure (Ji *et al*., 2014). Similarly, a three-band structure has also emerged for the zonally averaged GSST trend. The observable zonally averaged warming (>0.1 K since 1900) first took place in the subtropical regions of the Northern Hemisphere and 50°S of the Southern Hemisphere almost simultaneously, then followed by the subpolar warming in the Northern Hemisphere. The apparent warming emerged in both hemispheres around 1910 and the latitudinal scope of warming expanded towards the equator since then. As part of the Southern Hemisphere band, a sub-band was generated in tropical regions of the Southern Hemisphere around 1930 which can be identified by the tongue-like extensions of the contours towards the left-hand side. The 0.1 K lines of bands in both hemispheres joined at the equator by about 1970. For the subpolar band in the Northern Hemisphere, it was relatively narrow in meridional width and the zonally averaged warming lagged those of the former two bands. Zonally averaged warming at all latitudes accelerated from 1970 onwards, especially for the tropical oceans and subpolar regions in the Northern Hemisphere. Except for the slight northward shift in the Southern Hemisphere's band, the greatest warming regions in recent decades were stuck in the original first warming bands including subtropical regions in both hemispheres and subpolar regions in the Northern Hemisphere with the zonally averaged accumulated warming has exceeded 0.9 K from 1900. These greatest warming regions are associated with the enhanced warming over the global sub-tropical western boundary currents in both hemispheres and amplified warming in the Arctic Ocean, respectively. Though slight averaged cooling was found in the first decades over the equator, expansions from extratropical warming bands made the equator one of the fastest-warming regions in recent decades.

As the largest and deepest of Earth's oceanic divisions, the Pacific Ocean has significant impacts on global and regional climate and weather patterns. The

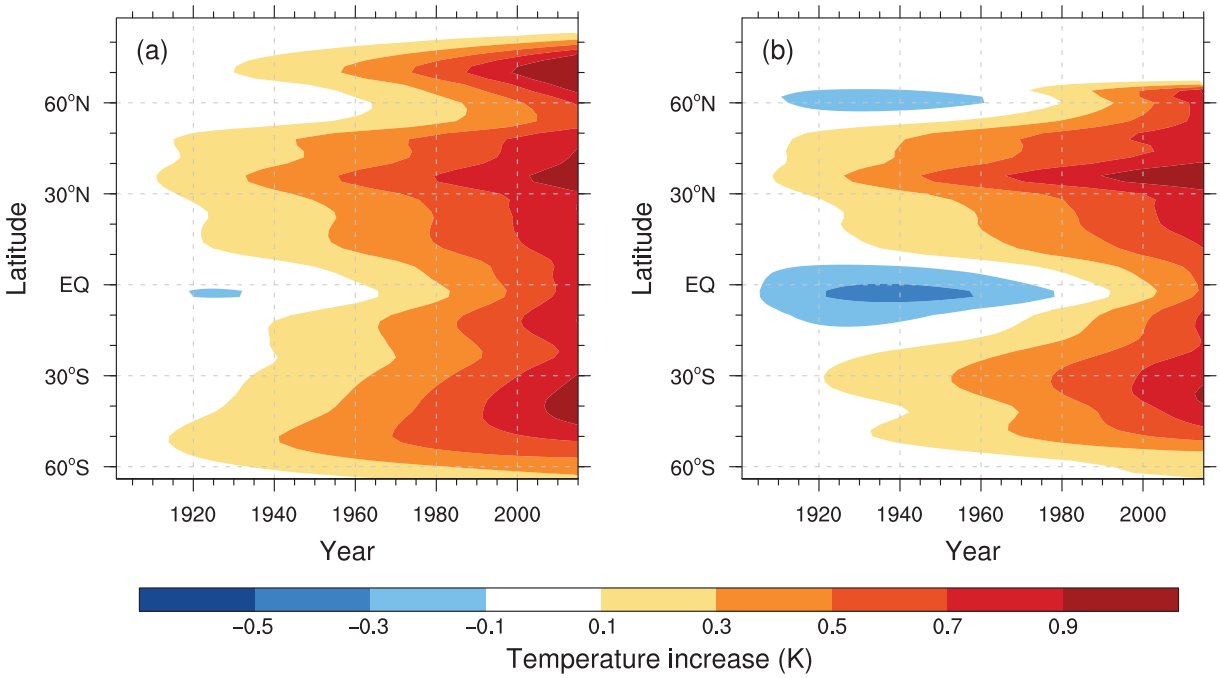


**FIGURE 3** Evolution of the zonally averaged trend of sea surface temperature. (a) The zonally averaged trend of global sea surface temperature. (b) The zonally trend of sea surface temperature of pan-Pacific (100°E–80°W, 65°S–65°E) [Colour figure can be viewed at wileyonlinelibrary.com]

connection between atmosphere and sea encompasses a broad range of timescales including The Madden–Julian oscillation (MJO), the largest element of the intra-seasonal (30- to 90-day) variability in the tropical atmosphere; ENSO in the tropical Pacific, pronounced at interannual timescales; PDO, a robust, recurring pattern of ocean–atmosphere climate variability centred over the mid-latitude Pacific basin, one of the representative modes of decadal variability, and so on. Owing to the importance and distinctiveness of the tropical Pacific showed before, we further investigated the evolution of the zonally averaged trend of SSTs over pan-Pacific, which is shown in Figure 3b. It is clearly found that warming started in both subtropical regions of the Pacific when cooling was restricted in narrow bands between 10°N and 10°S. With the equatorward propagation from the two warming bands, the cooling areas shrank quickly and turned into fast warming. Though the greatest warming is found to have occurred in subtropical regions no matter for global average or pan-Pacific, tropical regions, especially over central Pacific experienced the fastest-warming, except for subpolar regions, recently. The evolution of the zonally averaged warming rate is shown in Figure S15, from which the central Pacific is found to have undergone the most dramatic change: starting with the fastest cooling and ending with the fastest warming.

### 3.4 | Differences between the regional oceans

GSST trend has evolved as shown in Figures 1 and 2 and most of the global oceans have warmed under global warming. However, discrepancies between different oceans are remarkable, mainly reflected in the different speeds of warming in various regions or persistent cooling trends over some certain regions. Thus, we investigate the features of some regional oceans including the tropical central and eastern Pacific Ocean, east Southern Ocean, Indian Ocean, and North Atlantic Ocean.

The tropical central and eastern Pacific hosts a well-known climate mode of SST variability in terms of ENSO, which is a naturally occurring phenomenon and has global impacts of great relevance to society. The warming phase of the SST is known as El Niño while the opposite cold phase is La Niña. Anomalous warming (cooling) conditions are associated with a large-scale east–west sea level pressure seesaw, accompanied by weaker (stronger) Walker circulation and diminished (enhanced) trade winds than normal. The tropical trade winds are found to be weakened in the last century and would further decrease under a warmer climate in the 21st century (England *et al.*, 2014). However, an unprecedented strengthening of Pacific trade winds in the past two decades is suggested to have taken place by recent

high-quality observations. Various effects (such as the rapid sea-level rise and change of ocean currents) of this phenomenon were recorded (Timmermann *et al.*, 2010; Feng *et al.*, 2011) and mechanisms for that have been proposed (Luo *et al.*, 2012; McGregor *et al.*, 2014). One effect of the intensified Walker circulation is associated with sea surface cooling in the eastern Pacific, which has been identified as one of the contributors to the current global surface warming hiatus (Meehl *et al.*, 2013; England *et al.*, 2014). The current slowdown of global warming is thought to be part of natural climate variability (Kosaka and Xie, 2013) and a result of a downward decadal modulated oscillation combined with the secular warming trend (Huang *et al.*, 2017a; 2017b).

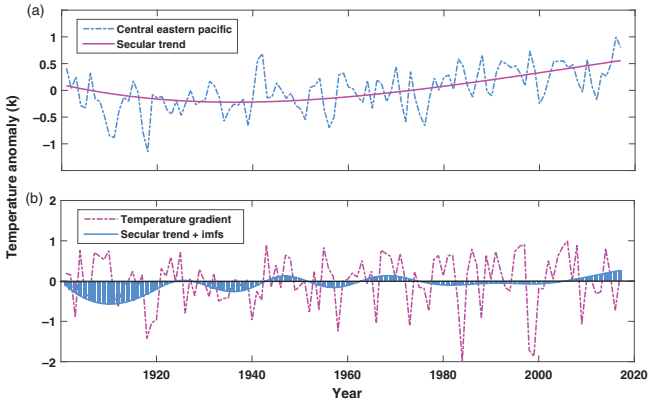


**FIGURE 4** Secular trend of the sea surface temperature anomaly of the tropical central and eastern Pacific and the temperature gradient. (a) The dashed blue line is the mean temperature anomaly of the central Eastern Pacific (20°S–14°N, 160°E–90°W), and the magenta line is the EEMD trend. (b), The dashed magenta line is the gradient between western Pacific Ocean (WP; 4°S–4°N, 160–180°E) and central eastern Pacific Ocean (EP; 4°S–4°N, 100–80°W) and the blue bar chart and line is the sum of the EEMD trend and the last two IMFs [Colour figure can be viewed at wileyonlinelibrary.com]

For the tropical central and eastern Pacific Ocean, the averaged SST is shown in Figure 4a. The corresponding linear trend demonstrates continuous warming for this region while the cooling trend over the first decades is ignored, but which is actually an unneglected phenomenon and can be captured by the EEMD trend. The secular trend shows a first cooling and latter warming with a turning point around 1950. When the last two IMFs which represent the multidecadal and decadal oscillations are added, decreasing of the SST in recent decades is demonstrated as the magenta line in Figure 4a. The temperature gradient between the west and the central eastern Pacific Ocean is also plotted in Figure 4b and the secular EEMD trend shows a slightly increasing trend. The amplitude of the decadal modulated oscillation is found to be decreasing during the last century. Over the recent three decades, the combined secular trend and decadal component show a remarkable warming trend, which is consistent with the intensified Walker circulation and strengthened of Pacific trade winds in the past two decades.

The lag − 1 autocorrelation coefficient of the averaged tropical central and eastern Pacific Ocean SST is $\alpha = .54$. With this lag − 1 autocorrelation coefficient, 5,000 red noise time series are generated and then decomposed by the EEMD method to derive their EEMD trends. Both thick black lines in Figure 5a are two-standard-deviation spread lines of the EEMD trend of 5,000 time-series. The red line in Figure 5a indicates the normalized EEMD trend of the averaged tropical central and

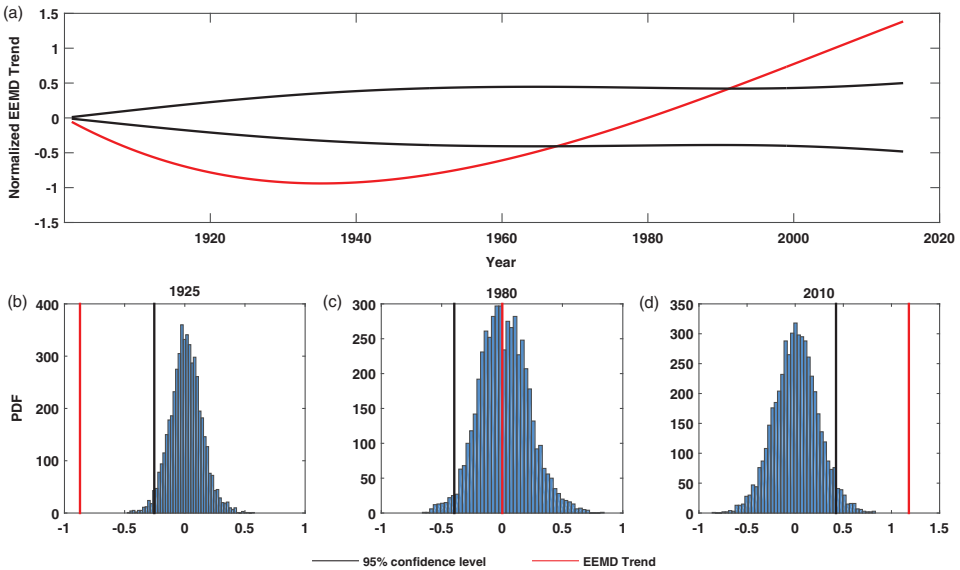


**FIGURE 5** Statistical significance test for EEMD trend of the sea surface temperature anomaly of the tropical central and eastern Pacific. (a) Two black lines are two-standard-deviation spread lines of EEMD trends for 5,000 red noise series with lag − 1 autocorrelation coefficient $\alpha = .55$. Red line denotes the normalized EEMD trend of the sea surface temperature anomaly of the tropical central and eastern Pacific. (b–d) The empirical probability density function (PDF) of the EEMD trends at the year 1925, 1980, and 2010, respectively [Colour figure can be viewed at wileyonlinelibrary.com]

eastern Pacific Ocean SST. To test the statistical significance of this trend, we compare it with the two-standard-deviation spread lines of the EEMD trend of the red background noise at each temporal location. If the former is beyond the spread line, the trend is then considered statistically significant. As shown in Figure 5a, the EEMD trend before 1970 and after 1990 of the averaged tropical central and eastern Pacific Ocean SST is statistically significant. Figure 5b–d present the comparison at three randomly selected years 1925, 1980, and 2010, respectively, in which the EEMD trend of the averaged tropical central and eastern Pacific Ocean SST is not statistically different from the trend of red background noise with 0.54 lag − 1 autocorrelation in 1980, but significantly different in 1925 and 2010. The statistical significance test described in Section 2.3.1 for IMFs is shown in Figure 6. The dashed lines are the theoretical spread lines of 90% (red) and 80% (blue) confidence levels. Therefore, after the temperature gradient between the west and the central eastern Pacific Ocean is decomposed into IMFs, the averaged period and corresponding energy can be compared with the reference lines to determine whether a specific IMF is statistically significant or not. It is clear from Figure 6 that IMF3 stays above 90% confidence level while IMF1 and IMF5 seem to contain some useful information, that is, they are bordering on the statistically significant at 80% confidence level. Meanwhile, the significance test for the EEMD trend of the temperature gradient between the west and the central eastern Pacific Ocean is shown in Figure S12a with lag − 1 autocorrelation coefficient $\alpha = .1$, and the increase in the EEMD trend is found to be statistically significant during the whole time span.

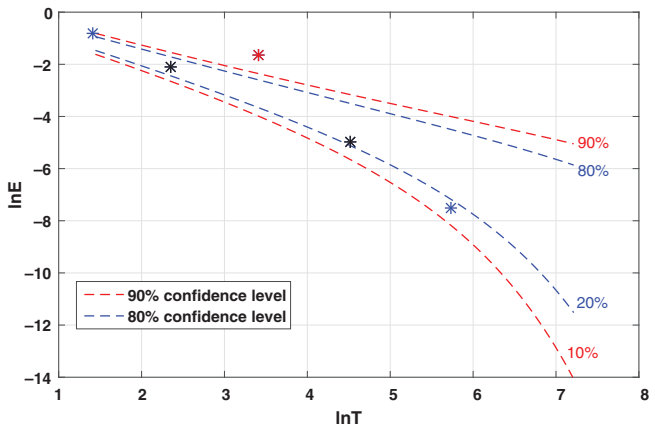


**FIGURE 6** Statistical significance test for IMFs of the sea surface temperature anomaly of the gradient between western Pacific Ocean (WP; 4°S–4°N, 160–180°E) and central eastern Pacific Ocean (EP; 4°S–4°N, 100–80°W) between the energy density (lnE) and the averaged period (lnT). Note that the marker stars from left to right indicate the energy density as a function of the averaged period [Colour figure can be viewed at wileyonlinelibrary.com]

Results aforementioned and studies referenced above have highlighted the roles that low frequency such as decadal and multidecadal oscillations played in modulating the centennial temperature trend. Therefore, it is critical to remove the influences of signals from other time scales when we focus on a specific component. By using MEEMD, Feng *et al.* (2014) defined an alternative Niño 3.4 index to reflect more on the interannual variability of equatorial Pacific SSTAs, examined each ENSO warm event they identified and SSTAs off Baja California were found to be a trigger of CP ENSO by a southwestward propagation. As a powerful naturally occurring phenomenon, ENSO exerts great impacts on the global climate. Substantial efforts have been made to understand and predict the physical properties, development, and links to other climate systems, thus ENSO is perhaps the one whose occurrence, dynamics, and influences have been relatively well understood and predicted (Yang *et al.*, 2018). However, ENSO changes as the global climate warming up and nontraditional ENSO conditions were observed during the last decades which were termed 'ENSO diversity'. The recent discovery of ENSO has some scientists believing it to be linked to global warming. However, there is no scientific consensus on how climate change might affect ENSO and whether these ENSO types are really distinct or are different manifestations of a continuum is currently under debate. More especially, limited information about future ENSO conditions can be provided by climate models make that how will ENSO change in the future climate a big challenging question. Therefore, taking advantage of the MEEMD method to emphasize oscillation on a specific time scale, to reveal the temporal–spatial evolution on naturally separated time scales, or even to generate an alternative reference framework for climate anomalies might provide a new perspective and be helpful to identify, describe, and understand the ENSO diversity.

As displayed before, the western Indian Ocean has undergone faster and stronger warming than the eastern part. To further investigate this issue, we calculate the mean SSTA of the western and eastern Indian Ocean and their corresponding EEMD trend as shown in Figure 7. Studies over the past two decades have been devoted to the cause and effect of the basin-wide Indian Ocean warming, which has shown that the entire Indian Ocean has been warming throughout the past half-century and the western tropical Indian Ocean has been warming for more than a century, at a rate faster than any other region of the tropical oceans, and turned out to be the largest contributor to the overall trend in the global mean SST (Roxy *et al.*, 2014). As shown in Figure 7, different

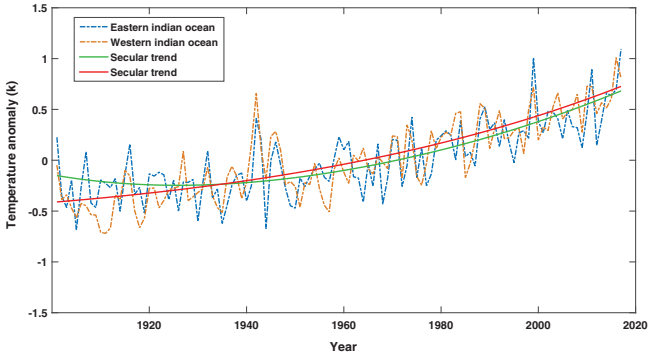


**FIGURE 7** Secular trend of the averaged sea surface temperature anomaly of the eastern (14°S–20°N, 100–120°E) and western (14°S–20°N, 50–70°E) Indian Ocean, respectively [Colour figure can be viewed at wileyonlinelibrary.com]

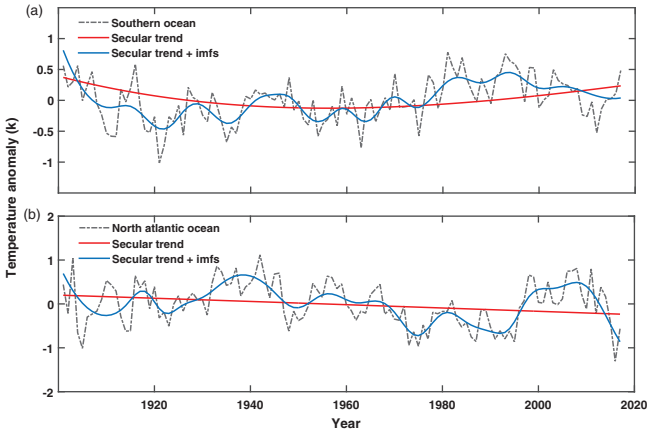


**FIGURE 8** EEMD fitting of the sea surface temperature anomaly of the Southern Ocean in the Pacific sector (46–64°S, 150–90°W) and North Atlantic Ocean (52–58°N, 32–26°W). (a), the dashed black line is the averaged sea surface temperature anomaly of the Southern Ocean, the magenta line is the secular trend and the blue line is the sum of the secular trend and last three IMFs. (b), same as Figure 6a but for the North Atlantic Ocean [Colour figure can be viewed at wileyonlinelibrary.com]

long-term trends of the western and eastern Indian Ocean are illustrated. A slight cooling trend is found before it turned into a warming trend around 1930 over the eastern Indian Ocean while continues warming is demonstrated over the western Indian Ocean, which is consistent with previous studies. Combined with the EEMD trend and warming rate evolution shown in Figures 1 and 2, it is clearly revealed that warming over the western Indian Ocean was faster than that of the eastern part during the first decades of last century and comparable to the eastern Indian Ocean for recent decades, though the magnitude of warming over the western Indian Ocean was greater than that of the eastern Indian Ocean. Significance tests for EEMD trend of eastern and western Indian Ocean SSTs are shown in Figure S12b,c with lag − 1 autocorrelation coefficient $\alpha = .61$ and .81, respectively. Warming over the eastern Indian Ocean is shown to be statistically significant during the last five decades while the whole time span for the western Indian Ocean. This condition closely resembles a positive Indian Ocean Dipole state which is characterized by anomalous warming in the western tropical Indian Ocean and cooling in the east. These positive IOD events have devastating impacts, including droughts in southeast China (Xu *et al.*, 2019) and Australia (Ummenhofer *et al.*, 2009), and flooding in East Africa (Behera *et al.*, 2005), as well as the Asian monsoon (Ashok *et al.*, 2001). Faster warming over the western Indian Ocean may result in more occurrences of stronger positive IOD events (Cai *et al.*, 2021), yet the reasons behind the prominent increasing trend of positive IOD events are still debated and many challenges still exist in assessing IOD responses and associated risks in a warming world (Abram *et al.*, 2020).

Two other regions with conspicuous features under global ocean warming are the Southern Ocean in the Pacific sector and the subpolar North Atlantic Ocean. The main feature of the evolution of SST's centennial trend in the Southern Ocean in the Pacific sector is identical to that in the central and eastern Pacific Ocean, both of which cooled first then turned into a warming trend around 1940 almost simultaneously, as shown in Figure 4a and 8a. The Southern Ocean is critical to the Earth's climate system by playing a role as a significant sink for heat and CO2, the world's most biologically productive ocean, and a site for the production of the coldest, densest water that is one of the dominant driving forces for the global overturning circulation (Liu and Curry, 2010). Attentions have been paid to this region by analysing the SST's trend. Different results were found while investigating different time intervals, which may lead to various physical interpretations. For instance, Liu and Curry (2010) found the observed SST in the Southern Ocean showed a substantial warming trend for the second half of the 20th century, while Haumann *et al.* (2020) illustrated that much of the Southern Ocean surface south of 55°S cooled and freshened between at least the early 1980s and the early 2010s and proposed that these trends were predominantly caused by an increased wind-driven northward sea-ice transport. These different warming and cooling trends are closely associated with different branches of a multidecadal oscillation from Figure 8a. When the low-frequency components including the multidecadal oscillation are extracted by EEMD, the more precisely fitted long-term trend captured the feature of first cooling and latter warming in

the Southern Ocean well. The significance test for the EEMD trend of SST over the Southern Ocean in the Pacific sector is shown in Figure S12d with lag − 1 autocorrelation coefficient $\alpha = .55$, which implies a significant change. The last two IMFs are thought to contain some useful information because they stay above 95% confidence level as illustrated in Figure S13a. Though the trend turned from cooling to warming, the temperature increase was still negative as shown in Figure 1. This trend differs from that over the north pole, which implies an asymmetry between the poles, and the ocean circulation is thought to play an important role in this phenomenon. Specifically, the deep water of the world ocean forms in the winter subpolar North Atlantic flows southward and upwells to the surface in the Southern Ocean (Marshall *et al*., 2014). The deep water that upwells in the Southern Ocean is free of the ongoing anthropogenic warming and then weakened the surface warming in the Southern Ocean. This asymmetry between the amplified Arctic warming and the muted surface warming over the Southern Ocean is born out in observations and confirmed by climate model simulations (Xie, 2020).

The other region with the noticeable feature of the global warming pattern is located in the subpolar North Atlantic Ocean where has been cooling during the time span. Generally, the main concern about the SST mode of North Atlantic is a warming/cooling variability on decadal timescales which has been termed as the Atlantic Multidecadal Oscillation/Atlantic Multidecadal Variability (AMO/AMV) (Schlesinger and Ramankutty, 1994). However, maps of temperature trends over the twentieth century show a persistent subpolar North Atlantic cooling, which is known as a 'warming hole' and has been widely believed to be linked to slow ocean processes especially a reduction in the Atlantic Meridional Overturning Circulation (AMOC) over the twentieth century and the melting of the Greenland Ice Sheet (Rahmstorf *et al*., 2015). Under greenhouse warming, the reduced northward heat transport by the AMOC slow down suppresses the ocean surface warming in the subpolar North Atlantic, and the disequilibrium with the warming atmosphere allows large ocean heat uptake (Xie, 2020). As shown in Figure 8b and Figure S13b, the averaged SST of North Atlantic has significant low-frequency variability and the secular trend extracted by EEMD confirms the cooling trend which is considerable after 1965 (Figure S12e with lag − 1 autocorrelation coefficient $\alpha = .57$).

## 4 | CONCLUSIONS AND DISCUSSIONS

In this study, the MEEMD method was applied to extract the long-term trend of GSST. By defining a nonlinear EEMD trend, we investigated how the GSST trend evolved at the centennial timescale and compared the different features between various oceans. It has been found that the detailed evolution of the GSST trend is non-uniform and different features are captured in different regions. Generally, the GSST EEMD trend in 2015 exhibit warming everywhere except the western of northern North Atlantic, the equatorial central Pacific, and the Southern Ocean in the Pacific sector. The subpolar North Atlantic Ocean has been cooling during the whole-time span while both the equatorial central Pacific and the Southern Ocean in the Pacific sector have undergone the first cooling and later warming. The now greatest warming occurs over the Arctic Ocean, east of the continents in the northern hemisphere, and the eastern tropical Atlantic Ocean. By taking advantage of the nature of the EEMD trend that varies with time and space, we also analysed the warming/cooling rate of SSTs trend. The results showed that the strongest warming during recent decades was in the Arctic Ocean, east of the continents in the northern hemisphere, the entire Indian Ocean, and especially in the tropical Pacific Ocean. The equatorial central Pacific Ocean has experienced the most dramatic changes during the last century while initially cooling trends turned into rapid warming with accelerated paces during recent decades. For zonally averaged GSST, a three-band structure has also emerged. The noticeable warming started in the subtropical regions of the Northern Hemisphere and 50°S of the Southern Hemisphere around 1915 and the latitudinal scope of warming expanded gradually towards the equator since then. Later around 1930, the subpolar warming in the Northern Hemisphere followed. Except for the slight northward shift in the Southern Hemisphere's band, the greatest warming regions in recent decades were stuck in the original first warming bands including subtropical regions in both hemispheres and subpolar regions in the Northern Hemisphere with the zonally averaged accumulated warming has exceeded 0.9 K from 1900.

The long-term trend evolution of SSTs from three other commonly used data sets are compared in Figures S1–S6. Generally, they exhibit broad similarity in their trend evolution patterns with discrepancies located in tropical central and eastern Pacific and Southern Ocean in the Pacific sector with smaller amplitude in COBE-SST and HadISST. To assess the uncertainties of the secular trend extracted by the EEMD method, we use the down sampling approach (Wu *et al*., 2011) discussed in Section 2.4. Figure S12 presents uncertainty estimates for tropical central and eastern Pacific; temperature gradient between western and central eastern the Pacific Ocean; eastern Indian Ocean; western Indian Ocean; the Southern Ocean in the Pacific sector and North Atlantic

Ocean. It is clear that the uncertainty towards two ends of the data range is relatively larger, which is understandable, as any temporally local analysis method suffers some degree of end-effect. However, the temporal locality of EEMD is smaller, and so are the uncertainties at the two ends compared with other methods, which has been discussed in the study of the uncertainty of the GSST (Wu *et al*., 2011).

The assessment of long-term trends and variability of SST is always suffering from large uncertainties for GSST reconstructed datasets especially early in the record and during the World War II. This limits the research for the climate system and makes it like a dilemma. Because the patterns of variability in any particular SST data set will depend on both the spatial and temporal resolution of the data and the length of the record. For instance, satellite-based SST archives of high spatial resolution but the short duration may reveal patterns with little information on multidecadal or longer timescale variability. Conversely, historical archives with long duration may reveal patterns with timescales of multiple decades and longer but lack detailed spatial information. The purpose of this work is to find how GSST evolved under global warming during the last century from a new perspective, which we believe would be important and helpful for understanding global climate change even in the slightest hint. Since the above evolution characteristics of the SST trend of centennial timescales were well demonstrated, questions then have been arisen. For example, we do not know why the western Indian Ocean warms faster and greater than the eastern part, or why the central Pacific Ocean has experienced the most dramatic change. Different features illustrated in different ocean basins may be tied to corresponding modes of climate variability such as ENSO, IOD, and AMO. These modes interact most readily via the atmosphere, through which modes in one ocean basin can be damped, enhanced, or even entirely generated by a mode in another ocean basin (Kajtar *et al*., 2017) and literature is rich on the interactions between modes of different ocean basins. The time-varying trend we defined in this study is capable to reveal how fast that one ocean would respond to global warming, which may provide a better understanding of these highly complex inter-basin interactions.

## ACKNOWLEDGEMENTS

This research was jointly supported by the National Science Foundation of China (41875083, 42075029, and 41705047) and Chinese Desert Meteorological Science Research Found (Sqj2019013). NOAA_ERSST_V5 data provided by the *NOAA/OAR/ESRL PSD*, *Boulder*, *Colorado*, *USA*, from their Web site at https://www.esrl.noaa.gov/psd/. The COBE-SST and Kaplan SST V2 data provided by the NOAA/OAR/ESRL PSL, Boulder, Colorado, USA, from their Web site at https://psl.noaa.gov/. The HadISST data can be found online (https://www.metoffice.gov.uk/hadobs/hadisst/data/download.html). Here, we also want to thank Taiwan's National Central University Research Center analysis of data for producing and making available the fast EEMD code.

## ORCID

*Fei Ji* https://orcid.org/0000-0002-7985-1558

## REFERENCES

Abram, N.J., Gagan, M.K., Cole, J.E., Hantoro, W.S. and Mudelsee, M. (2008) Recent intensification of tropical climate variability in the Indian ocean. *Nature Geoscience*, 1, 849–853.

Abram, N.J., Wright, N.M., Ellis, B., Dixon, B.C., Wurtzel, J.B., England, M.H., Ummenhofer, C.C., Philibosian, B., Cahyarini, S.Y., Yu, T.-L., Shen, C.-C., Cheng, H., Edwards, R. L. and Heslop, D. (2020) Coupling of indo-pacific climate variability over the last millennium. *Nature*, 579, 385.

Ashok, K., Guan, Z.Y. and Yamagata, T. (2001) Impact of the Indian ocean dipole on the relationship between the Indian monsoon rainfall and ENSO. *Geophysical Research Letters*, 28, 4499–4502.

Behera, S.K., Luo, J.J., Masson, S., Delecluse, P., Gualdi, S., Navarra, A. and Yamagata, T. (2005) Paramount impact of the Indian ocean dipole on the east African short rains: a CGCM study. *Journal of Climate*, 18, 4514–4530.

Brown, P.T., Li, W., Cordero, E.C. and Mauget, S.A. (2015) Comparing the model-simulated global warming signal to observations using empirical estimates of unforced noise. *Scientific Reports*, 5 (1), 1–9.

Cai, W., Cowan, T. and Raupach, M. (2009) Positive Indian ocean dipole events precondition southeast Australia bushfires. *Geophysical Research Letters*, 36(19). https://doi.org/10.1029/2009GL039902.

Cai, W., Yang, K., Wu, L., Huang, G. and Yamagata, T. (2021) Opposite response of strong and moderate positive Indian ocean dipole to global warming. *Nature Climate Change*, 11, 27–32.

Cai, W.-J., Hu, X., Huang, W.-J., Murrell, M.C., Lehrter, J.C., Lohrenz, S.E., Chou, W.-C., Zhai, W., Hollibaugh, J.T., Wang, Y., Zhao, P., Guo, X., Gundersen, K., Dai, M. and Gong, G.-C. (2011) Acidification of subsurface coastal waters enhanced by eutrophication. *Nature Geoscience*, 4, 766–770.

Chen, C.-T.A., Lui, H.-K., Hsieh, C.-H., Yanagi, T., Kosugi, N., Ishii, M. and Gong, G.-C. (2017a) Deep oceans may acidify faster than anticipated due to global warming. *Nature Climate Change*, 7, 890.

Chen, X., Zhang, X., Church, J.A., Watson, C.S., King, M.A., Monselesan, D., Legresy, B. and Harig, C. (2017b) The increasing rate of global mean sea-level rise during 1993–2014. *Nature Climate Change*, 7, 492.

Cheng, L., Abraham, J., Zhu, J., Trenberth, K.E., Fasullo, J., Boyer, T., Locarnini, R., Zhang, B., Yu, F., Wan, L., Chen, X., Song, X., Liu, Y. and Mann, M.E. (2020) Record-setting ocean

warmth continued in 2019. *Advances in Atmospheric Sciences*, 37, 137–142.

Cohen, J., Screen, J.A., Furtado, J.C., Barlow, M., Whittleston, D., Coumou, D., Francis, J., Dethloff, K., Entekhabi, D., Overland, J. and Jones, J. (2014) Recent arctic amplification and extreme mid-latitude weather. *Nature Geoscience*, 7, 627–637.

Deser, C., Alexander, M.A., Xie, S.-P. and Phillips, A.S. (2010a) Sea surface temperature variability: patterns and mechanisms. *Annual Review of Marine Science*, 2, 115–143.

Deser, C., Phillips, A.S. and Alexander, M.A. (2010b) Twentieth century tropical sea surface temperature trends revisited. *Geophysical Research Letters*, 37(10). https://doi.org/10.1029/2010GL043321.

Deutsch, C., Brix, H., Ito, T., Frenzel, H. and Thompson, L. (2011) Climate-forced variability of ocean hypoxia. *Science*, 333, 336–339.

England, M.H., McGregor, S., Spence, P., Meehl, G.A., Timmermann, A., Cai, W., Sen Gupta, A., McPhaden, M.J., Purich, A. and Santoso, A. (2014) Recent intensification of wind-driven circulation in the pacific and the ongoing warming hiatus. *Nature Climate Change*, 4, 222–227.

Feng, J., Wu, Z. and Zou, X. (2014) Sea surface temperature anomalies off Baja California: a possible precursor of ENSO. *Journal of the Atmospheric Sciences*, 71, 1529–1537.

Feng, M., Boening, C., Biastoch, A., Behrens, E., Weller, E. and Masumoto, Y. (2011) The reversal of the multi-decadal trends of the equatorial pacific easterly winds, and the Indonesian Throughflow and Leeuwin Current transports. *Geophysical Research Letters*, 38(11). https://doi.org/10.1029/2011GL047291.

Franzke, C. (2009) Multi-scale analysis of teleconnection indices: climate noise and nonlinear trend analysis. *Nonlinear Processes in Geophysics*, 16, 65–76.

Giese, B.S., Compo, G.P., Slowey, N.C., Sardeshmukh, P.D., Carton, J.A., Ray, S. and Whitaker, J.S. (2010) The 1918/19 El Nino. *Bulletin of the American Meteorological Society*, 91, 177–183.

Haumann, F.A., Gruber, N. and Münnich, M. (2020) Sea-ice induced southern ocean subsurface warming and surface cooling in a warming climate. *AGU Advances*, 1(2), e2019AV000132. https://doi.org/10.1029/2019AV000132.

Hu, Z.-Z., Huang, B., Kinter, J.L., III, Wu, Z. and Kumar, A. (2012) Connection of the stratospheric QBO with global atmospheric general circulation and tropical SST. Part II: interdecadal variations. *Climate Dynamics*, 38, 25–43.

Huang, B., Thorne, P.W., Banzon, V.F., Boyer, T., Chepurin, G., Lawrimore, J.H., Menne, M.J., Smith, T.M., Vose, R.S. and Zhang, H.-M. (2017a) Extended reconstructed sea surface temperature, version 5 (ersstv5): upgrades, validations, and intercomparisons. *Journal of Climate*, 30, 8179–8205.

Huang, J., Xie, Y., Guan, X., Li, D. and Ji, F. (2017b) The dynamics of the warming hiatus over the northern hemisphere. *Climate Dynamics*, 48, 429–446.

Huang, N.E., Shen, Z., Long, S.R., Wu, M.L.C., Shih, H.H., Zheng, Q.N., Yen, N.C., Tung, C.C. and Liu, H.H. (1998) The empirical mode decomposition and the Hilbert spectrum for nonlinear and non-stationary time series analysis. *Proceedings of the Royal Society a-Mathematical Physical and Engineering Sciences*, 454, 903–995.

Huang, N.E. and Wu, Z. (2008) A review on Hilbert-Huang transform: method and its applications to geophysical studies. *Reviews of Geophysics*, 46(2). https://doi.org/10.1029/2007RG000228.

IPCC. (2013) *Climate change 2013: The physical science basis. Contribution of working group I to the fifth assessment report of the intergovernmental panel on climate change*. In: Stocker, T.F., Qin, D., Plattner, G.-K., Tignor, M., Allen, S.K., Boschung, J., Nauels, A., Xia, Y., Bex, V., and Midgley, P.M. (Eds.). Cambridge, UK and New York, NY: Cambridge University Press, 1535 pp. doi:https://doi.org/10.1017/CBO9781107415324.

IPCC. (2019) Summary for policymakers. *IPCC special report on the ocean and cryosphere in a changing climate*. Pörtner, H.O., Roberts, D.C., Masson-Delmotte, V., Zhai, P., Tignor, M., Poloczanska, E., Mintenbeck, K., Alegría, A., Nicolai, M., Okem, A., Petzold, J., Rama, B., Weyer, N.M. (Eds.). In press.

Ishii, M., Shouji, A., Sugimoto, S. and Matsumoto, T. (2005) Objective analyses of sea-surface temperature and marine meteorological variables for the 20th century using ICOADS and the KOBE collection. *International Journal of Climatology*, 25, 865–879.

Ji, F., Wu, Z., Huang, J. and Chassignet, E.P. (2014) Evolution of land surface air temperature trend. *Nature Climate Change*, 4, 462–466.

Kajtar, J.B., Santoso, A., England, M.H. and Cai, W. (2017) Tropical climate variability: interactions across the Pacific, Indian, and Atlantic oceans. *Climate Dynamics*, 48, 2173–2190.

Kaplan, A., Cane, M.A., Kushnir, Y., Clement, A.C., Blumenthal, M.B. and Rajagopalan, B. (1998) Analyses of global sea surface temperature 1856-1991. *Journal of Geophysical Research-Oceans*, 103, 18567–18589.

Kosaka, Y. and Xie, S.-P. (2013) Recent global-warming hiatus tied to equatorial pacific surface cooling. *Nature*, 501, 403.

Kulp, S.A. and Strauss, B.H. (2019) New elevation data triple estimates of global vulnerability to sea-level rise and coastal flooding. *Nature Communications*, 10(1), 1–12.

Liu, J. and Curry, J.A. (2010) Accelerated warming of the southern ocean and its impacts on the hydrological cycle and sea ice. *Proceedings of the National Academy of Sciences of the United States of America*, 107, 14987–14992.

Luo, J.-J., Sasaki, W. and Masumoto, Y. (2012) Indian ocean warming modulates pacific climate change. *Proceedings of the National Academy of Sciences of the United States of America*, 109, 18701–18706.

Marshall, J., Armour, K.C., Scott, J.R., Kostov, Y., Hausmann, U., Ferreira, D., Shepherd, T.G. and Bitz, C.M. (2014) The ocean's role in polar climate change: asymmetric arctic and Antarctic responses to greenhouse gas and ozone forcing. *Philosophical Transactions of the Royal Society a-Mathematical Physical and Engineering Sciences*, 372, 20130040.

McGregor, S., Timmermann, A., Stuecker, M.F., England, M.H., Merrifield, M., Jin, F.-F. and Chikamoto, Y. (2014) Recent walker circulation strengthening and pacific cooling amplified by Atlantic warming. *Nature Climate Change*, 4, 888–892.

Meehl, G.A., Covey, C., Delworth, T., Latif, M., McAvaney, B., Mitchell, J.F.B., Stouffer, R.J. and Taylor, K.E. (2007) The WCRP CMIP3 multimodel dataset—a new era in climate change research. *Bulletin of the American Meteorological Society*, 88, 1383–1394.

Meehl, G.A., Hu, A., Arblaster, J.M., Fasullo, J. and Trenberth, K.E. (2013) Externally forced and internally generated decadal climate variability associated with the interdecadal pacific oscillation. *Journal of Climate*, 26, 7298–7310.

Qian, C., Wu, Z., Fu, C. and Zhou, T. (2010) On multi-timescale variability of temperature in China in modulated annual cycle reference frame. *Advances in Atmospheric Sciences*, 27, 1169–1182.

Rahmstorf, S., Box, J.E., Feulner, G., Mann, M.E., Robinson, A., Rutherford, S. and Schaffernicht, E.J. (2015) Exceptional twentieth-century slowdown in Atlantic Ocean overturning circulation. *Nature Climate Change*, 5, 475–480.

Rayner, N.A., Parker, D., Horton, E.B., Folland, C., Alexander, L., Rowell, D., Kent, E. and Kaplan, A. (2003) Global analyses of sea surface temperature, sea ice, and night marine air temperature since the late nineteenth century. *Journal of Geophysical Research*, 108(D14). https://doi.org/10.1029/2002JD002670.

Roxy, M.K., Ritika, K., Terray, P. and Masson, S. (2014) The curious case of Indian ocean warming. *Journal of Climate*, 27, 8501–8509.

Schlesinger, M.E. and Ramankutty, N. (1994) An oscillation in the global climate system of period 65-70 years. *Nature*, 367, 723–726.

Screen, J.A., Deser, C. and Simmonds, I. (2012) Local and remote controls on observed arctic warming. *Geophysical Research Letters*, 39(10). https://doi.org/10.1029/2012GL051598.

Stroeve, J.C., Serreze, M.C., Holland, M.M., Kay, J.E., Malanik, J. and Barrett, A.P. (2012) The Arctic's rapidly shrinking sea ice cover: a research synthesis. *Climatic Change*, 110, 1005–1027.

Timmermann, A., McGregor, S. and Jin, F.-F. (2010) Wind effects on past and future regional sea level trends in the southern indo-pacific. *Journal of Climate*, 23, 4429–4437.

Trenberth, K.E., Fasullo, J.T. and Balmaseda, M.A. (2014) Earth's energy imbalance. *Journal of Climate*, 27, 3129–3144.

Ummenhofer, C.C., England, M.H., McIntosh, P.C., Meyers, G. A., Pook, M.J., Risbey, J.S., Gupta, A.S. and Taschetto, A.S. (2009) What causes southeast Australia's worst droughts? *Geophysical Research Letters*, 36(4). https://doi.org/10.1029/2008GL036801.

Vecchi, G.A., Clement, A. and Soden, B.J. (2008) Examining the tropical Pacific's response to global warming. *Eos Transactions American Geophysical Union*, 89, 81–83.

Wang, Y.-H., Yeh, C.-H., Young, H.-W.V., Hu, K. and Lo, M.-T. (2014) On the computational complexity of the empirical mode decomposition algorithm. *Physica A: Statistical Mechanics and Its Applications*, 400, 159–167.

Webster, P.J., Holland, G.J., Curry, J.A. and Chang, H.R. (2005) Changes in tropical cyclone number, duration, and intensity in a warming environment. *Science*, 309, 1844–1846.

Wei, M., Qiao, F., Guo, Y., Deng, J., Song, Z., Shu, Q. and Yang, X. (2019) Quantifying the importance of interannual, interdecadal and multidecadal climate natural variabilities in the modulation of global warming rates. *Climate Dynamics*, 53, 6715–6727.

Wu, L., Cai, W., Zhang, L., Nakamura, H., Timmermann, A., Joyce, T., McPhaden, M.J., Alexander, M., Qiu, B., Visbeck, M., Chang, P. and Giese, B. (2012) Enhanced warming over the global subtropical western boundary currents. *Nature Climate Change*, 2, 161–166.

Wu, Z. and Huang, N.E. (2009) Ensemble empirical mode decomposition: a noise-assisted data analysis method. *Advances in Adaptive Data Analysis*, 01, 1–41.

Wu, Z., Huang, N.E. and Chen, X. (2009) The multi-dimensional ensemble empirical mode decomposition method. *Advances in Adaptive Data Analysis*, 1(3), 339–372.

Wu, Z., Huang, N.E., Long, S.R. and Peng, C.-K. (2007) On the trend, detrending, and variability of nonlinear and nonstationary time series. *Proceedings of the National Academy of Sciences of the United States of America*, 104, 14889–14894.

Wu, Z., Huang, N.E., Wallace, J.M., Smoliak, B.V. and Chen, X. (2011) On the time-varying trend in global-mean surface temperature. *Climate Dynamics*, 37, 759–773.

Wu, Z.H. and Huang, N.E. (2004) A study of the characteristics of white noise using the empirical mode decomposition method. *Proceedings of the Royal Society a-Mathematical Physical and Engineering Sciences*, 460, 1597–1611.

Xie, S.P. (2020) Ocean warming pattern effect on global and regional climate change. *AGU Advances*, 1(1), e2019AV000130. https://doi.org/10.1029/2019AV000130.

Xu, C., An, W., Wang, S.Y.S., Yi, L., Ge, J., Nakatsuka, T., Sano, M. and Guo, Z. (2019) Increased drought events in southwest China revealed by tree ring oxygen isotopes and potential role of Indian ocean dipole. *Science of the Total Environment*, 661, 645–653.

Yang, S., Li, Z., Yu, J.-Y., Hu, X., Dong, W. and He, S. (2018) El Nino-southern oscillation and its impact in the changing climate. *National Science Review*, 5, 840–857.

Yao, S.-L., Luo, J.-J., Huang, G. and Wang, P. (2017) Distinct global warming rates tied to multiple ocean surface temperature changes. *Nature Climate Change*, 7, 486.

Zhang, M. and Song, H. (2006) Evidence of deceleration of atmospheric vertical overturning circulation over the tropical pacific. *Geophysical Research Letters*, 33(12). https://doi.org/10.1029/2006GL025942.

## SUPPORTING INFORMATION

Additional supporting information may be found online in the Supporting Information section at the end of this article.

**How to cite this article:** Xu Z, Ji F, Liu B, *et al.* Long-term evolution of global sea surface temperature trend. *Int J Climatol*. 2021;1–15. https://doi.org/10.1002/joc.7082